Long-acting nanoparticle-loaded bilayer microneedles for protein delivery to the posterior segment of the eye

Wu, Y., Vora, L. K., Wang, Y., Adrianto, M. F., Tekko, I. A., Waite, D., Donnelly, R., & Thakur , R. R. S. (2021). Long-acting nanoparticle-loaded bilayer microneedles for protein delivery to the posterior segment of the eye. *European Journal of Pharmaceutics and Biopharmaceutics*, *165*, 306-318. https://doi.org/10.1016/j.ejpb.2021.05.022

Published in:
European Journal of Pharmaceutics and Biopharmaceutics

Document Version:
Peer reviewed version

Long-acting nanoparticle-loaded bilayer microneedles for protein delivery to the posterior segment of the eye

Yu Wu[a], Lalitkumar K. Vora[a], Yujing Wang[a], Muhammad Faris Adrianto[a, b], Ismaiel A. Tekko[a, c], David Waite[a], Ryan Donnelly [a], Raghu Raj Singh Thakur [a, *]

a. School of Pharmacy, Medical Biology Centre, Queen's University Belfast, 97 Lisburn Road, Belfast BT9 7BL, UK
b. Department of Pharmaceutical Chemistry, Faculty of Pharmacy, Airlangga University, Surabaya, East Java, 60115, Indonesia
c. Faculty of Pharmacy, Aleppo University, Aleppo, Syria

*Corresponding author. Tel: +44 (0) 28 9097 5814. Email: r.thakur@qub.ac.uk.

** Corresponding Author*

Dr Thakur Raghu Raj Singh
Reader in Pharmaceutics
School of Pharmacy
Queen's University Belfast
Medical Biology Centre
97 Lisburn Road
Belfast, BT9 7BL
United Kingdom
Tel: +44 (0) 28 9097 5814
Email: r.thakur@qub.ac.uk

ABSTRACT

Treatment of neovascular ocular diseases involves intravitreal injections of therapeutic proteins using conventional hypodermic needles every 4-6 weeks. Due to the chronic nature of these diseases, these injections will be administrated to patients for the rest of their lives and their frequent nature can potentially pose a risk of sight-threatening complications and poor patient compliance. Therefore, we propose to develop nanoparticle (NP)-loaded bilayer dissolving microneedle (MN) arrays, to sustain delivery of protein drugs in a minimally invasive manner. In this research, a model protein, ovalbumin (OVA)-encapsulated PLGA NPs were prepared and optimised using a water-in-oil-in-water (W/O/W) double emulsion method. The impact of stabilisers and primary sonication time on the stability of encapsulated OVA was evaluated using an enzyme-linked immunosorbent assay (ELISA). Results showed that the lower primary sonication time was capable of sustaining release (77 days at 28.5% OVA loading) and improving the OVA bioactivity. The optimised NPs were then incorporated into a polymeric matrix to fabricate bilayer MNs and specifically concentrated into MN tips by high-speed centrifugation. Optimised bilayer MNs exhibited good mechanical and insertion properties and rapid dissolution kinetics (less than 3 min) in excised porcine sclera. Importantly, *ex vivo* transscleral distribution studies conducted using a multiphoton microscope confirmed the important function of MN arrays in the localisation of proteins and NPs in the scleral tissue. Furthermore, the polymers selected to prepare bilayer MNs and OVA NPs were determined to be biocompatible with retinal cells (ARPE-19). This delivery approach could potentially sustain the release of encapsulated proteins for more than two months and effectively bypass the scleral barrier, leading to a promising therapy for treating neovascular ocular diseases.

Keywords: Nanoparticle, Bilayer microneedle, posterior segment, long-acting drug delivery, ocular delivery

1. Introduction

Diseases of the posterior segment of the eye such as age-related macular degeneration (AMD) and diabetic retinopathy are rapidly increasing and challenging to treat [1,2]. Currently, several anti-VEGF agents such as ranibizumab (Lucentis®), bevacizumab (Avastin®), aflibercept (Eylea®) and brolucizumab (Beovu®) are used in treating these diseases. However, it is challenging to deliver these biomacromolecules to the back of the eye due to their large size and the eye's complicated anatomical structure. Conventional methods such as topical (e.g., eye drop) and systemic (e.g., oral tablets) administrations to the eye are associated with low bioavailability (< 5%) and systemic side-effects, respectively. These challenges are especially significant for posterior segment ocular drug delivery due to the physiological barriers (e.g., sclera, cornea, choroid), longer diffusion pathways and the vitreous body's cellular nature [3]. Therefore, direct injections in the eye *via* hypodermic needles are used to deliver the macromolecules into the vitreous cavity to achieve sufficient concentrations within the target tissue, which is often the retina.

Typically, the most common therapy for neovascular ocular disorders is the intravitreal injection of anti-VEGF agents [4]. However, due to these diseases' chronic and progressive natures, repeated injections are required to maintain the therapeutic level in the choroid/retina [5]. Conventional injections not only induce pain and discomfort to the patients but may also lead to the risk of severe complications such as cataracts, retinal detachment, and elevation of intraocular pressure [6]. The transscleral route is gaining increased interest as a promising and efficient route for posterior segment disease treatment due to its large surface area, variable thickness, and the shorter diffusion pathway to the target tissue [7]. Furthermore, it is less invasive than an intravitreal injection, as transscleral delivery occurs around the outer surface of the eye [2]. Macromolecules have to diffuse across the sclera, a dense connective tissue, before reaching the target site [8], but the physicochemical properties (e.g., molecular weight/radius, solubility and charge) of macromolecules restrict effective permeability across the sclera, resulting in low intraocular bioavailability [9,10]. Accordingly, these barriers and limitations of existing treatments have raised the demand for novel delivery systems, with sustained-release profiles to deliver macromolecules to the back of the eye efficiently.

Several systems have been developed to enhance the therapeutic delivery to the posterior segment of the eye. These approaches can be classified into two types: bioavailability

enhancement approaches and modified drug delivery systems. Firstly, bioavailability enhancement approaches such as topical gels, contact lenses, and ocular inserts showed an incremental improvement for small molecules but little progress with macromolecules [11,12]. On the other hand, device-based penetration enhancing approaches to enhance ocular bioavailability such as iontophoresis, ultrasound, and microneedles (MNs) are gaining interest [13,14]. As a patient-friendly administration device, MNs provide numerous benefits, including efficient barrier penetration, minimally invasiveness, ease of application, commercial feasibility and potentially enhanced therapeutic efficacy [15,16]. Among various MN types, the dissolving MN is a promising approach as it eliminates the risk of accidental tissue damage, induced by brittle solid or hollow MNs, minimises biohazard wastage and is easy to scale-up at a low cost [17–20]. Secondly, modified drug delivery systems such as long-acting systems (e.g., implants [21] and micro/nano-particles) have been developed to sustain the release of drugs[22]. Nanoparticles (NPs) can provide various advantages, such as shielding encapsulated biomacromolecules from the physiological environment, controlling the release rate of the molecules, reducing dosing frequency, achieving target delivery and enhancing the permeability of the payload [23–25].

In this research project, we combined two technologies, NPs in dissolving MNs, and made a hybrid system to deliver biomacromolecules/proteins to the eye in a minimally invasive approach. PLGA-based NPs were fabricated to sustain the release, while the dissolving MNs offer enhanced delivery of biomacromolecules to the posterior ocular tissue. To minimise drug wastage, the bilayer MN structure was employed, where the NPs were mainly concentrated in the tip part. Ovalbumin (OVA, 44 kDa) was selected as the model protein owing to its similar molecular weight to that of the anti-VEGF drug – ranibizumab (48 kDa) [26]. OVA NP-loaded bilayer MNs were developed to achieve efficient delivery of OVA to the posterior segment of the eye in a sustained and minimally invasive manner.

2. Materials and methods

2.1 Materials

Ovalbumin (OVA), poly (vinyl alcohol) (PVA) (31-50 kDa), poly (vinyl alcohol) (PVA) (12-23 kDa), (2-Hydroxypropyl)-β-cyclodextrin (HP-β-CD), polyethylene glycol 400 (PEG 400), dimethyl sulfoxide (DMSO) and dichloromethane (DCM) were purchased from Sigma-Aldrich (Basingstoke, UK). Poly(vinyl pyrrolidone) (PVP) (58 kDa) was obtained from Ashland

(Kidderminster, UK). Poly (D, L-lactide-co-glycolide) (PLGA 5002A, 50:50 copolymer ratio, MW 17 kDa) was supplied by Corbion Biomedical, UK. Trehalose dihydrate and mannitol (purity, 99%) were purchased from Alfa Aesar (Lancashire, UK). All other chemicals were of analytical grade and purchased from standard suppliers.

2.2 Preparation of OVA-encapsulated PLGA NPs

OVA-encapsulated PLGA NPs were prepared by the water-in-oil-in-water（W/O/W) double emulsion solvent evaporation method, as described by Zaric *et al.* with specific modifications [27]. As shown in Fig. 1, to prepare the primary W/O emulsion, 100 μL of OVA in phosphate buffer saline (PBS) (pH 7.4) was emulsified in a PLGA solution (20 mg PLGA in 700 μL DCM) using a probe sonicator (Sonics & Materials VC50, Danbury, USA), at a power of 50 W. The obtained W/O emulsion was added dropwise into 7 mL PVA solution (2.5% w/v) under mild stirring, then probe sonication was employed to obtain a W/O/W double emulsion. All sonication processes were operated under cold conditions, through the use of an ice bath. The prepared emulsion was stirred overnight to evaporate its organic solvent. Next, in order to remove excess PVA and un-encapsulated OVA, NPs were harvested and washed three times with deionised water by centrifugation (Eppendorf® 5804 series centrifuge, Fisher Scientific, Loughborough, UK) at 17,000 g, at 4°C for 20 min. The collected NPs were pre-frozen at a -80°C freezer for 2 h and then lyophilised by a freeze drier (Virtis Advantage Bench-top Freeze-drier system, SP Scientific, Warminster, PA, USA). The lyophilisation cycle utilised is presented in Table S1. For fluorescein isothiocyanate-labelled OVA (FITC-OVA) encapsulated NPs, the same procedure was repeated in dark conditions.

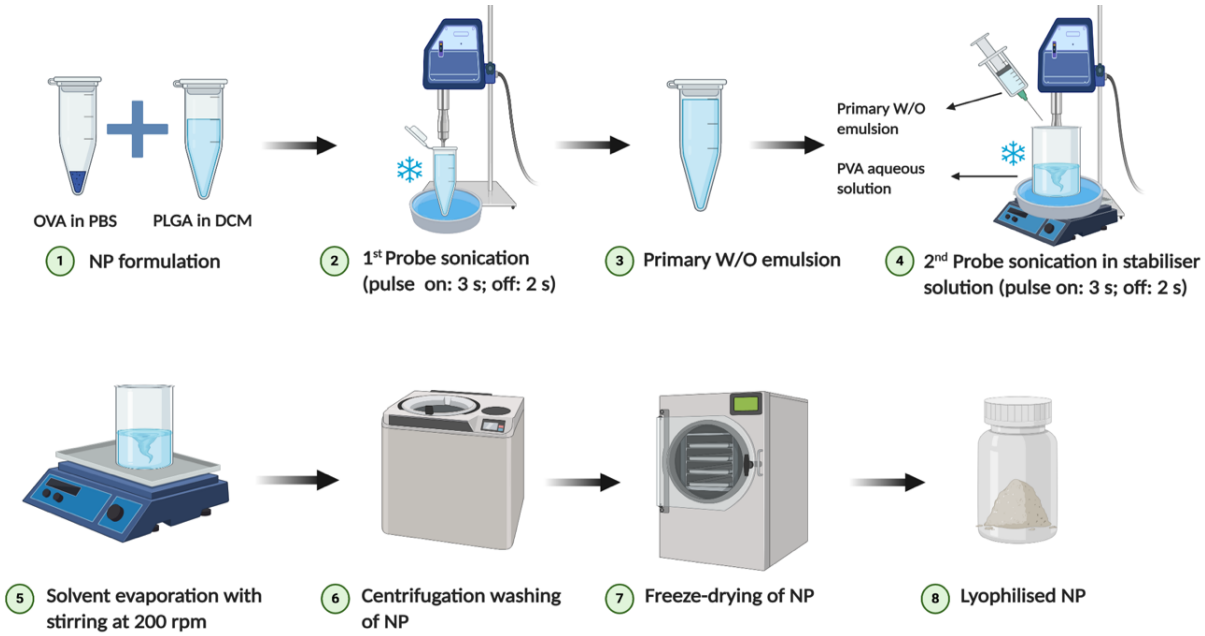

Fig. 1. Schematic representation of the fabrication process of OVA-encapsulated PLGA NPs by W/O/W double emulsion solvent evaporation method.

2.3 Optimisation of NP formulation

To achieve a suitable particle size and high drug content in the formulation, the effect of three manufacturing conditions – the concentration of OVA in the inner aqueous phase, the primary sonication time and the secondary sonication time – on several particle properties, namely particle size, polydispersity index (PDI), encapsulation efficiency (EE) and loading capacity (LC) were investigated. Different parameters involved in the fabrication of OVA NPs are summarised in Table 1.

Table 1. Different parameters used to fabricate OVA-encapsulated PLGA NPs

OVA concentration (% w/v)	Primary sonication time (sec)	Secondary sonication time (sec)
4	30	60
8	30	60
12	30	60
20	30	60
12	10	10
12	10	30
12	10	60
12	60	60

2.4 Physicochemical properties of NPs

Dynamic light scattering (DLS) (ZetaSizer® Nanoseries ZS system, Malvern Instruments, Worcestershire, UK) was used to measure the hydrodynamic radius, polydispersity index and zeta potential of the optimised NPs before and after lyophilisation. The lyophilised powder of NP was resuspended in distilled water and diluted to a suitable concentration for particle size and zeta potential analysis. All measurements were carried out in triplicate. The morphology and shape of the OVA NPs were evaluated by a transmission electron microscope (TEM) (JEOL JEM 1400-plus transmission electron microscope, Japan, JEOL UK, Welwyn Garden City, UK) with an accelerating voltage of 120 kV. To this end, the water diluted sample with a suitable concentration was dropped on a copper grid coated with Formvar film, for TEM observation.

To quantify the %EE and %LC of OVA in prepared PLGA NPs, 5 mg of lyophilised NPs were dissolved in a mixture of 15% v/v DMSO, 85% v/v 50 mM NaOH and 0.5% w/v sodium dodecyl sulfate (SDS), which can accelerate the hydrolysis of the polymer [28]. After overnight incubation, a clear solution was obtained, allowing the concentration of OVA to be determined using a Micro Bicinchoninic Acid (BCA) protein assay kit (Thermo Scientific™, Loughborough, UK). The standard calibration curves were also prepared in the mixture of DMSO, NaOH and SDS. The %EE and %LC of OVA encapsulated in PLGA NPs were calculated using Eq. (1) and Eq. (2), respectively.

$$\%EE = \frac{\text{Amount of OVA entrapped}}{\text{Total amount of OVA used for encapsulation}} \times 100\ \% \quad (1)$$

$$\%LC = \frac{\text{Amount of OVA entrapped}}{\text{Total amount of nanoparticles}} \times 100\ \% \quad (2)$$

2.5 Recovery of OVA from the primary W/O emulsion

In order to enhance the bioactivity of OVA during the harsh conditions of the W/O/W emulsion fabrication method, several additives were added to the formulation. Primary sonication time was also reduced to determine its effect on the stabilisation of OVA during the preparation of the primary W/O emulsion, which is considered as the major factor responsible for protein destabilisation [29,30]. The detailed operation was described by Sah *et al.* with specific modifications [31]. Briefly, OVA solution was added into DCM and the probe sonication was applied to emulsify the mixture, with parameters the same as described in Section 2.2. As shown in Table 2, various additives (e.g., HP-β-CD, PEG 400, trehalose and mannitol) at different concentrations were added to the OVA solution and the duration of primary sonication was modulated to detect their influence on OVA recovery from the primary W/O emulsion, in the absence of PLGA. In this process, OVA was extracted from DCM by adding 10 mL PBS and then centrifuged at 3,000 g for 20 min to speed up the phase separation. The emulsion prepared by a 30-sec probe sonication, without additives, was selected as the control group. The recovery of extracted OVA from primary emulsion was quantified by a Micro BCA protein assay and calculated using Eq. (3).

$$\text{OVA recovery (\%)} = \frac{\text{Amount of OVA detected after emulsification}}{\text{Total amount of OVA}} \times 100\ \% \quad (3)$$

Table 2. Different parameters used to study the effect of sonication time and additives on OVA recovery from primary W/O emulsion in the absence of PLGA.

Sample	OVA concentration (% w/v)	Additive (% w/v)	Sonication time (sec)
Control	12	—	30
F1	12	HP-β-CD 10	30
F2	12	HP-β-CD 30	30
F3	12	PEG 400 10	30
F4	12	PEG 400 30	30
F5	12	Mannitol 10	30
F6	12	Mannitol 30	30
F7	12	Trehalose 10	30
F8	12	Trehalose 30	30
F9	12	—	60
F10	12	—	10

205 *2.6 In vitro release of OVA from PLGA NPs*

206

207 *In vitro* release profiles of OVA NPs were carried out by dispersing 5 mg of lyophilised OVA
208 NPs in 1 mL PBS (pH 7.4, 0.05% w/v sodium azide) and incubating at 37 °C with mild shaking
209 (40 rpm). At predetermined time intervals, the suspensions were centrifuged into a pellet and
210 500 μL of the supernatant was collected and replaced with pre-warmed fresh release medium.
211 The OVA concentration and bioactivity in the collected supernatant were quantified by a Micro
212 BCA assay and a direct enzyme-linked immunosorbent assay (ELISA), respectively. OVA and
213 a mixture of OVA and PLGA with the same loading of 5 mg OVA NPs were also incubated in
214 the same release medium and recorded as negative (control-) and positive control (control+),
215 respectively.

216

217 *2.7 Fabrication of protein-encapsulated NPs-loaded bilayer dissolving MNs*

218

219 Several formulations have been tested to optimise the MNs, to deliver a greater payload. The
220 compositions of various formulations are listed in Table 3. The manufacturing method of the
221 bilayer dissolving MNs is illustrated in Fig. 2. Initially, lyophilised OVA NPs were mixed
222 homogeneously with various aqueous gels using a speed mixer (SpeedMixer™ DAC 150.1
223 FVZ-K, High Wycombe, UK). Subsequently, 10 μL of the mixture was poured onto a laser-
224 engineered silicone conical mould (3 × 3 MN arrays, 750 μm height, 300 μm base width and
225 50 μm interspacing) to fill the mould microprojections by applying positive pressure (5 bar for
226 3 min) using a positive pressure chamber (Protima AT10 pressure tank, Richmond Scientific,
227 Lancashire, UK). After recovering the excess mixture, high-speed centrifugation (5,000 rpm,
228 15 min) was applied to concentrate NPs to the tips of MN arrays. After overnight drying, the
229 baseplate layer consisting of only the aqueous gel was added by slight centrifugation (3,000
230 rpm, 3 min). MN arrays were then dried at room temperature for 24 h and carefully removed
231 from the mould for further characterisation. The FITC-OVA NP-loaded dissolving MNs were
232 fabricated by the same method in dark conditions.

233

234

235

Table 3. Composition of the various formulations used to prepare OVA NP-loaded bilayer MNs.

Formulation	Lyophilised NP (% w/w)	PVA 31-50 kDa (% w/w)	PVP 58 kDa (% w/w)	Water (% w/w)
M1	20	10	10	60
M2	25	10	10	55
M3	30	10	10	50
M4	30	0	20	50
M5	40	0	20	40
M6	25	20	0	55

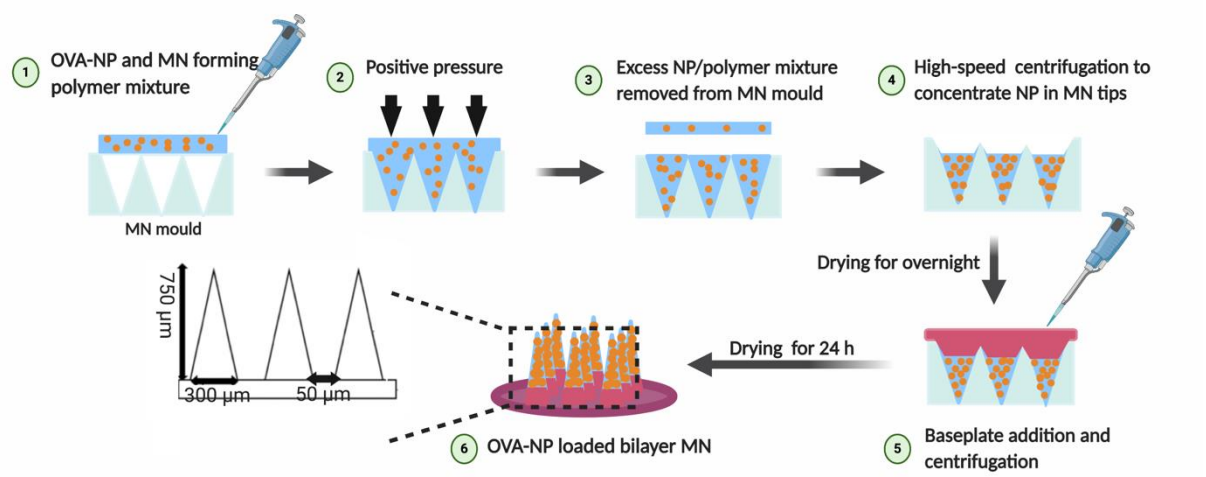

Fig. 2. Schematic representation of the preparation of OVA NP-loaded bilayer MN arrays.

2.8 Analytical methods

Quantification of OVA was conducted using a Micro BCA protein kit by following the enclosed protocol and the absorbance was detected by a multi-mode microplate reader (FLUOstar Omega, BMG Labtech) at 562 nm. The bioactivity of OVA was determined by a direct ELISA method. Initially, 100 µL of OVA standards and samples were coated into each well of a high-binding 96-well plate, covered with parafilm M® (Bemis Inc., Soignies, Belgium) and kept in the fridge at 8 °C overnight. The plate was then washed three times with 200 µL washing buffer, containing 0.05% v/v Tween 20 in PBS, after which, the plate was dried by tapping it vigorously on absorbent paper. The plate was then blocked with 1% w/v bovine serum albumin (BSA) and washed again with washing buffer as described previously. Afterwards, 100 µL antibody (rabbit polyclonal antibody conjugated with biotin) diluted in blocking buffer at the ratio of 1:5,000 was loaded and covered with parafilm. After a 40 min

incubation at room temperature, the plate was washed again with washing buffer. 100 µL of enzyme streptavidin-horseradish peroxidase with 10,000 times dilution in PBS was pipetted to each well and further incubated for 30 min at room temperature. After washing three times, 100 µL of 3,3',5,5'-tetramethylbenzidine (TMB) substrate was loaded into the plate. The plate was covered with aluminium foil and incubated at room temperature for 40 min until a blue colour developed. Absorbance at 650 nm was measured using the microplate reader.

2.9 Microscopy analysis of bilayer MN arrays

Both OVA NP-loaded bilayer MNs and FITC-OVA NP-loaded bilayer MNs were observed using a Leica EZ4D digital light microscope (Leica Microsystems, Milton Keynes, UK) to detect the structure and integrity of the bilayer MN arrays. A TM3030 benchtop scanning electron microscopy (SEM) (Hitachi, Tabletop Microscope, UK) was used to detect the surface morphology of bilayer MN arrays. In addition, an inverted Leica DM5500B fluorescence microscope (Leica Microsystems, Milton Keynes, UK) was used to collected widefield fluorescence images of FITC-OVA NP-loaded bilayer MNs to detect the distribution of NPs within the MN arrays. Samples were excited with 405 nm or 480 nm and fluorescence emissions were collected between 470 ± 40 nm and 527 ± 30 nm.

2.10 Mechanical, insertion and dissolution properties of NP-loaded MNs

The mechanical test was conducted by TA-XT2 Texture Analyser (Stable Microsystems, Haslemere, UK) in compression mode, as described previously, with a small modification [32,33]. Briefly, MN arrays were compressed under a 3 N force for 30 sec and the heights of the MN arrays before and after compression were measured using the digital light microscope. The reduction of height after compression was calculated using Eq. (4).

$$\text{Reduction in MN height (\%)} = \frac{\text{Initial height of MN array} - \text{Height of MN array after compression}}{\text{Initial height of MN array}} \times 100\ \% \quad (4)$$

Porcine scleral tissue was used as a scleral model to detect the insertion depth of NP-loaded MNs. Briefly, the bilayer MN was inserted into the sclera by the Texture Analyser at the required force of 3 N and held for 30 sec. One layer of Parafilm M® was used to separate the

MN array from the tissue to prevent the MN from rapid dissolution. The insertion depth of MN arrays into the scleral tissue was ascertained by optical coherence tomography (OCT) (EX 1301 OCT microscope, Michelson Diagnostics, Kent, UK) and analysed by ImageJ® (National Institutes of Health, Bethesda, USA). The dissolution study of the bilayer MNs was also conducted in porcine scleral tissues and the detailed operation was the same as described previously [32].

2.11 Quantification of OVA content localised in the MN tips

In order to determine the OVA content in each bilayer MN array, the baseplate of the MN array was held by a custom-made device and only the tip part was immersed in a mixture of DMSO and NaOH/SDS for several minutes until all the tips had dissolved. Afterwards, the drug content in the tips of the bilayer MN arrays was quantified using a Micro BCA kit, in triplicate.

2.12 Ex vivo drug distribution studies

Ex vivo distribution of FITC-OVA, administered as an eye drop and using bilayer MN arrays, was evaluated in the excised scleral tissue, using a modified Franz-diffusion cell set up. Briefly, the receptor chamber was filled with 5 mL of pre-warmed PBS buffer and the excised porcine sclera (with average thickness around 735.6 ± 48.83 μm) was mounted on the donor chamber as shown in Fig. 3. A volume of 50 μL FITC-OVA NP suspension, FTIC-OVA-loaded MN arrays and FITC-OVA NP-loaded bilayer MN arrays, with the same drug loading, were applied to the scleral tissues by pipetting or finger pressure. After 3 min of application, the MN arrays were removed from the scleral tissue. The scleral tissues were collected from the Franz-diffusion apparatus and rinsed with PBS and blotted dry after specific time intervals (1, 6 and 24 h). Next, the obtained scleral tissues were snap-frozen with liquid nitrogen and imaged by a multiphoton microscope (MPM) (Leica TCS SP8-multiphoton excited fluorescence upright microscope, Leica Microsystems Ltd., Milton Keynes, UK) to observe the distribution of drug inside the scleral tissue after the application of eye drops, plain drug-loaded MN arrays and NP-loaded MN arrays.

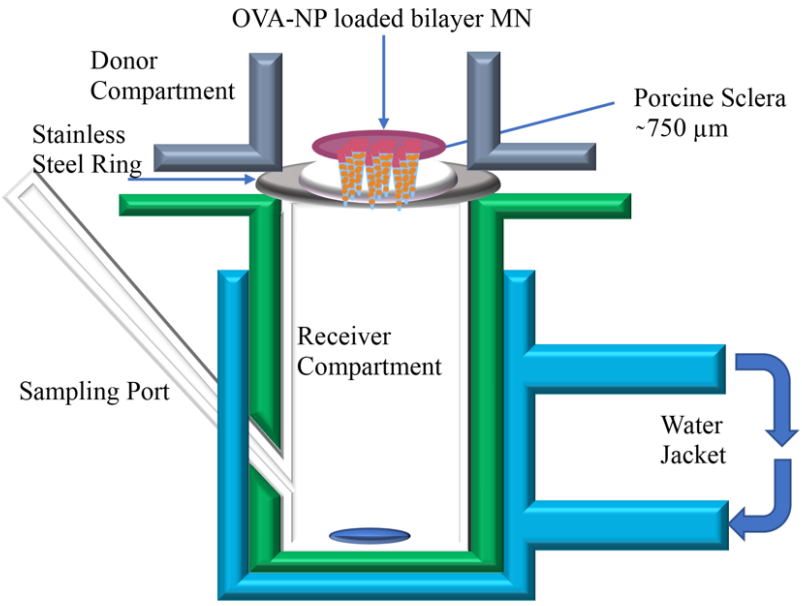

Fig. 3. Schematic representation of the modified Franz-diffusion cell set up for *ex vivo* drug distribution study using the porcine sclera as a scleral model.

2.13 Biocompatibility studies

For biocompatibility studies, the human retinal pigment epithelial (ARPE-19) cells were used to test any cytotoxicity due to the polymers (e.g., PVP 58 kDa, PLGA 5002A, PVA 12-23 kDa) and the OVA NPs. Initially, PVA, PVP and OVA NPs at various concentrations were dissolved in Dulbecco's phosphate buffer saline (DPBS) separately, whereas PLGA was firstly dissolved in DCM and DPBS was added after the evaporation of DCM. The obtained polymer solutions and NP suspension were filtered using 0.2 µm filters and diluted with cell culture medium in the equivalence of 1 to 100 times of them in each NP-loaded MN array. ARPE-19 cells were seeded into the 96-well tissue culture plate and after 48 h of incubation, the culture medium was removed and replaced with 200 µL filtered samples. After a further 24 h of incubation, 10 µL resazurin sodium salt solution was added to each well and the plates were incubated for another 4 h. The mean absorbance of the untreated group was recorded as 100% and the cell viability of the sample was obtained as a percentage of the untreated group.

2.14 Statistical analysis

The results were stated as mean ± standard deviation (SD) of the mean. The data was analysed using Microsoft Excel and GraphPad Prism® version 8 (GraphPad Software, San Diego, California, USA). Where appropriate, statistical comparisons were studied using the one-way analysis of variance (ANOVA). A difference was denoted as being statistically significant when the *p*-value was less than 0.05 and probability values were recorded as * = $p < 0.05$, ** = $p < 0.01$, *** = $p < 0.001$.

3. Results and discussion

3.1 Characterisation and optimisation of OVA NPs

OVA-loaded PLGA NPs were prepared by the most commonly used industrially scalable W/O/W double emulsion solvent evaporation technique [34]. Several formulation factors were optimised to prepare NPs with uniform size and morphology in addition to having the highest possible loading efficiency. As shown in Fig. 4A, the variation in OVA concentration had a limited influence ($p > 0.1$) on particle size, which ranged between 200-250 nm and PDI (< 0.2), indicating the uniformity of NPs. In contrast, an increase in initial OVA concentration considerably affected ($p < 0.01$) the loading efficiency of prepared NPs. According to Fig. 4B, with the drug concentration increasing from 0 to 12% w/v, the %EE of OVA within NPs decreased while the %LC increased significantly ($p < 0.01$). This is probably due to the higher concentration gradient of OVA between the inner and outer aqueous phase, leading to a higher loss of OVA to the external aqueous phase, thereby lowering the %EE [35]. However, after increasing the drug content from 12% to 20% w/v, %EE was significantly reduced from 73.69 ± 5.8% to 59.21 ± 3.96% ($p < 0.05$) whilst the improvement of %LC was not significant ($p > 0.05$). This indicated that the drug loading at 12% w/v was already saturated in the polymer matrix. Therefore, 12% w/v OVA was selected as the optimal concentration for further investigation.

After optimising the drug concentration, the physical characteristics of OVA NPs at different primary (0, 10, 30 and 60 sec) and secondary sonication times (10, 30 and 60 sec) were studied. The duration of primary sonication did not affect the particle size and PDI of OVA NPs (Fig. 4C). However, the primary sonication was found to be a necessary step to encapsulate OVA into PLGA NPs, as shown in Fig. 4D. The group without primary sonication resulted in

lower %EE (2.78 ± 0.32%) and %LC (0.19 ± 0.05%), but prolonging the primary sonication significantly ($p < 0.001$) increased both %EE and %LC. This indicated the importance of a stable primary emulsion in enhancing the loading efficiency of PLGA NPs, fabricated by the W/O/W solvent evaporation method. This might be caused by the high hydrophilicity of the drug. After being added to the outer aqueous phase, the unencapsulated highly water-soluble protein drugs tend to diffuse into the external aqueous phase and consequently are washed away [36,37]. Conversely, the duration of secondary sonication showed a limited effect ($p > 0.1$) on %EE of PLGA NPs (Fig. 4F), while it played a crucial role in adjusting the particle size and PDI. As shown in Fig. 4E, the longer secondary sonication time resulted in smaller and more homogenous NPs. At least 60 sec of secondary sonication was found to be sufficient to fabricate homogeneous OVA NPs, with a PDI of < 0.2. This observation was consistent with data reported by Son *et al.*, where the secondary sonication time was described as the dominant factor affecting the size and PDI of PLGA NPs [38].

379

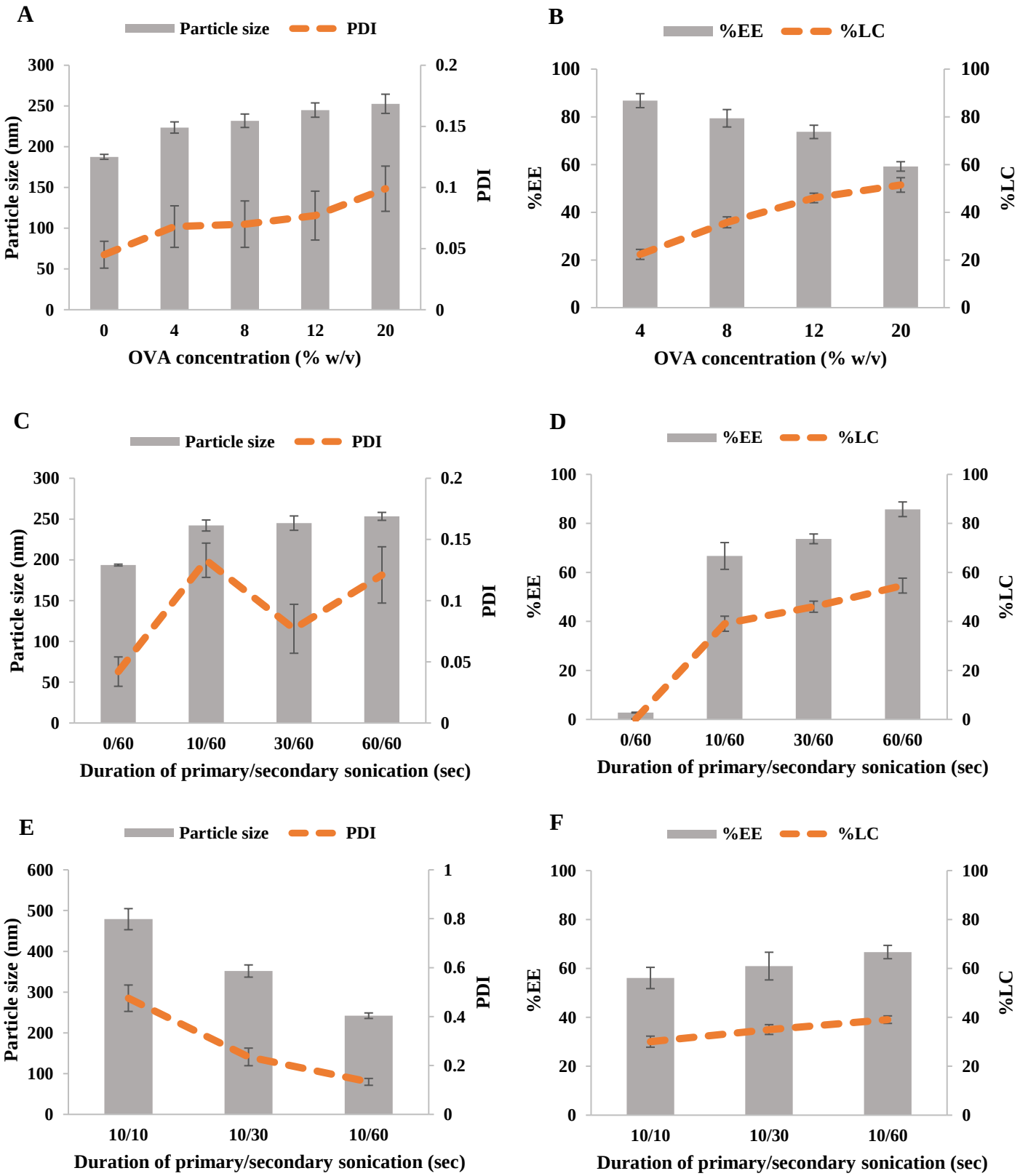

380 **Fig. 4.** Effect of different parameters on OVA NP characteristics: effect of OVA concentrations on (A) particle
381 size and PDI (B) %EE and %LC; effect of primary sonication time on (C) particle size and PDI (D) %EE and %LC;
382 effect of secondary sonication time on (E) particle size and PDI (F) %EE and %LC (mean ± SD, n=3).

3.2 Recovery of OVA from the primary emulsion

The stability of biomacromolecules during encapsulation into NPs has been a thorny issue, especially when using the W/O/W double emulsion solvent evaporation method. In this process, the biotherapeutics have to be exposed to high shear stress [39], temperature gradients induced by probe sonication, as well as organic solvents, which are all likely to induce detrimental effects on protein bioactivity. According to Jiang *et al.*, most of the deformation of the protein happened during the primary emulsification step of preparing a W/O emulsion [40]. Moreover, Hongkee *et al.* also proved that the aggregation and denaturation of OVA at the water/DCM interface was one of the main factors for the reduction of protein stability during the primary emulsification process [31]. During this process, the attractive force and interaction between the organic solvent and the hydrophobic area of proteins result in interfacial absorption, accompanied by unfolding and structural rearrangement of biomacromolecules [37,41,42]. Thus, the recovery of OVA from primary W/O emulsion was analysed to evaluate the protein stability. However, highly disruptive extract media (e.g., DCM or DMSO) used to destroy the emulsion could induce irreversible conformational changes of encapsulated proteins. So far, there is no method to extract proteins entirely from the primary W/O emulsion in the presence of PLGA without destabilisation of proteins [43–45]. Furthermore, the performance of protein recovery techniques is generally poor, due to the addition of excess buffer, which is likely to precipitate the PLGA with encapsulated proteins [43,46–48]. Based on these considerations, the primary emulsion was prepared in the absence of PLGA to investigate the influence of several additives and primary sonication time on protein recovery. Kang *et al.* proved that the emulsification without PLGA in the organic phase is feasible to reflect protein stability at the W/O interface in a fast and economic manner [45].

Several excipients such as sugars, PEG and cyclodextrins were added to the primary emulsion to stabilise the protein, either by competing with proteins to absorb at the W/O interface or accumulating at the interface, to protect proteins from exposure to the harsh environment, and consequently minimising the likelihood of the interfaced-induced protein aggregation [49]. Morlock *et al.* had substantiated that the aggregation of erythropoietin was reduced by adding cyclodextrins. The aromatic rings in cyclodextrins were supposed to shield the hydrophobic chains in proteins and increase their hydrophilicity [30]. Similarly, PEG 400 acting as a surfactant may minimise the penetration of protein in the interfacial film of W/O emulsions, as well as limiting the contacts of protein with the organic phase, and consequently, stabilise it

during primary emulsification [50]. However, in our case, there was no big difference between the groups with the addition of stabilisers (F1-F8) and the control group, as indicated in Fig. 5. The addition of sugars (mannitol and trehalose) (F5-F8) had a limited effect on improving the degree of OVA recovery, possibly due to the fact that the sugars used here are not surface active and have a limited affinity to the W/O interface, which is in agreement with other studies [31,51]. In contrast to our findings, previous studies claimed that HP-β-CD and PEG 400 at high concentration induced a protective function towards the protein during the preparation of the primary emulsion, but resulted in low protein loading efficiency [30,31,50]. In our study, after reducing the primary sonication time from 30 to 10 sec (F10), the recovery of OVA from primary W/O emulsion was enhanced substantially from 47.72 ± 3.96% to 81.57 ± 5.68%. This was possibly due to the reduction of primary sonication time, limiting the exposure of the protein to the organic phase, as well as shear stress and consequently, restricting the destabilising effects of the W/O interface. Furthermore, the protein is likely to behave as a self-protectant at high concentrations, thus minimising the detrimental influence of the W/O interface [29,52]. Therefore, the reduction of primary sonication time was identified to be a way to stabilise biomacromolecules during the primary W/O emulsion preparation.

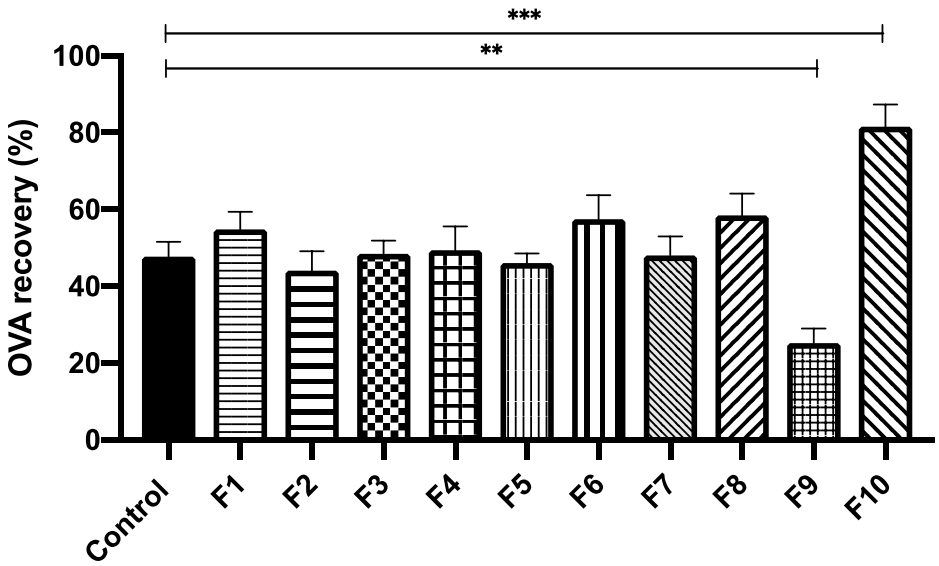

Fig. 5. The degree of OVA recovery from primary W/O emulsion fabricated by adding various additives of different concentrations and various duration of sonication (mean ± SD, n=3).

3.3 The characteristics of OVA NPs

The characteristics (i.e., size, PDI and zeta potential) of the optimised OVA NPs before and after lyophilisation are presented in Table S2. The results revealed that there was no significant difference ($p > 0.05$) in particle behaviours between lyophilised and non-lyophilised NPs. This result is consistent with several papers in which it was demonstrated that, due to the amorphous nature of lyophilised PLGA, resists in protein degradation thereby freeze-drying-induced protein denaturation is limited in PLGA particles [50-52].

TEM was used to investigate the morphology of OVA NPs. The optimised NPs exhibited spherical shapes with diameters around 200 nm (Fig. 7A), which was much smaller ($p < 0.05$) than those detected by DLS (242.1 nm). Since the DLS determines the NP diameters in a liquid state, which reflects the hydrodynamic radius, including the core plus any molecules attached *via* various non-covalent interactions, whereas TEM detects the actual size of NPs in the dried form [54,55]. Moreover, DLS is an intensity-based measurement and is very sensitive to large particles, thus tends to result in a larger size than TEM, which is a number-based particle size measurement.

3.4 In vitro release of OVA from PLGA NPs

The kinetics of the release of biotherapeutics from NPs play a critical role in clinical application. Therefore, after different time intervals, both the total and active amounts of OVA released from NPs fabricated by different primary sonication times were investigated. The ratio between them was recorded as the %bioactivity of released OVA. Due to the unique degradation property of PLGA, the encapsulated protein always be released in a triphasic profile [56,57]. As shown in Fig. 6A, all groups exhibited a mean burst release (24 h) of 3.1%, 3.31%, and 3.99% of OVA from the groups with 60, 30, 10 sec primary sonication times, respectively. The burst release could be due to surface-bound OVA [57]. In the next stage, the release rate was slower and almost linear against time, as the physically encapsulated protein gradually released through roundabout channels in the PLGA NPs. Herein, the group with reduced primary sonication time (10 sec) had a higher release rate than those with longer primary sonication time (30 and 60 sec), suggesting that the reduction of primary sonication time may markedly improve the release rate of OVA from NPs. By day 77, approximately 8%, 14.5% and 28.5%

of encapsulated OVA were released from the groups with 60, 30 and 10 sec primary sonication times, respectively.

Fig. 6B indicates the bioactivity of released protein. It was found that the duration of primary sonication time also exhibited a critical influence on the stability of the released protein. After reducing the sonication time from 60 to 10 sec, the %bioactivity of released OVA was markedly increased from approximately 30% to 60%. This result was consistent with the investigation of OVA from the primary W/O emulsion, in which the recovery of OVA was considerably improved after shortening the primary sonication time (Fig. 5). This is possibly due to the fact that the longer sonication time results in the protein being exposed to longer periods under both mechanical stress (shear stress) and chemical stress (organic solvent) [58]. Although numerous studies have shown the successful encapsulation of proteins into PLGA particles with suitable size and loading capacity, the incomplete release of proteins due to protein instability is still recognised as a major problem [40,58]. Generally, the methods for solving these problems can be divided into two categories: adding excipients and modifying the fabrication process, which were all tried in these studies. It was concluded that the release and bioactivity of OVA could be significantly improved by reducing the primary sonication time.

The results of the control groups indicated that after 77 day-incubation, both the %bioactivity of OVA in negative and positive control groups was maintained at a high level, thereby eliminating the possibility of protein instability induced by long-term incubation in PBS at 37 °C and the degradation of PLGA. Contrary to these findings, some other investigations have reported that the released protein was associated with stability issues due to the acidic microenvironment caused by the accumulation of acidic degradation products of PLGA [59,60]. Herein, possibly due to the limited amount of PLGA in OVA NPs, no severe influence on OVA stability was detected. Furthermore, Fu *et al.* have reported that the pH change within the delivery system also depends on the size of the carrier [62]. The pH issue induced by PLGA degradation typically happens in large-volume delivery systems (e.g. tablets, implants and microparticles) [52,62,63]. In these systems, the degradation of PLGA was proven to be faster on the inside due to the polymer degrading by hydrolysis in an acid-catalysed fashion, thereby forming an acidic environment within the carrier and denaturing the encapsulated protein. On the contrary, in NPs, due to their relatively small size and large surface area, clearance of acidic

degradation products is faster and the internal pH is easily neutralised by PBS, thus maintaining the bioactivity of the encapsulated protein [62].

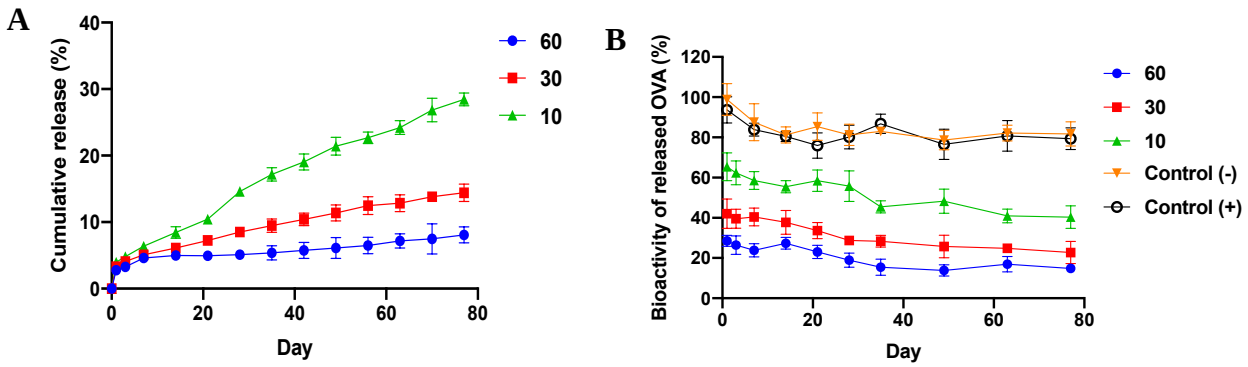

Fig. 6. (A) *In vitro* release profiles of OVA from PLGA NP fabricated from various durations of primary sonication (60, 30, 10 sec). (B) %Bioactivity of released OVA fabricated from various durations of primary sonication and also the %bioactivity of OVA in control groups (mean ± SD, n=3).

3.5 Fabrication of OVA NP-loaded dissolving bilayer MN arrays

The morphology and structure of fabricated bilayer MNs, as well as the distribution of NPs in MN array, were examined by a light microscope, SEM, and a fluorescence microscope. All observations showed that the bilayer MN arrays fabricated from all formulations had intact and sharp needles, with heights of approximately 750 µm. The light microscopic image of FITC-OVA NP-loaded MN (Fig. 7C) indicated the double-layered structure of MN arrays, suggesting NPs are specifically localised at the tips of MN array. Additionally, fluorescence microscopic images (Fig. 7E, F) further demonstrated that all FITC-OVA NPs were specifically deposited in tips, as there was a discrete line between green coloured tips, resulting from FITC-OVA encapsulated NPs and the blue bottom owing to the plain polymer matrix. Practically, due to the viscoelasticity of biological tissues and the weak mechanical properties of dissolving MNs, it is difficult to achieve full insertion of dissolving MNs into the scleral tissue within a few minutes, and consequently, a mass of drug will be lost, resulting in a lower drug delivery efficiency [65]. Herein, the bilayer structure of MNs was introduced to precisely localise cargos into MN tips and ultimately minimise cargo waste, as well as to enhance drug delivery efficiency, which is a profound benefit, due to being more cost-effective for delivering expensive anti-VEGF agents. Furthermore, as quantified by Micro BCA, 24.86 ± 2.01 µg of OVA was successfully encapsulated into each bilayer MN patch and the calculated release amount of OVA from each MN patch was approximately 90 ng/day. Herein, OVA was used

as the model protein of ranibizumab, which has an IC_{50} value of 11-27 ng/mL [66]. Based on the IC_{50} value and the volume of the human vitreous humour (4.4 ml), a total of 48.4-118.8 ng would be enough for limiting VEGF-A-induced endothelial cell proliferation [67]. Additionally, as reported by Malik *et al*., as an FDA-approved treatment for wet AMD, ranibizumab has a much higher toxicity level than bevacizumab and aflibercept, and it has been shown to be safe for human RPE cell viability even at ten-times normal clinical concentrations (5 mg) [68]. Overall, with ranibizumab having such a low IC_{50} as well as a broad safety profile there is no doubt that the amount of OVA released by bilayer MN arrays would be therapeutically effective and non-toxic even upon accumulation over time.

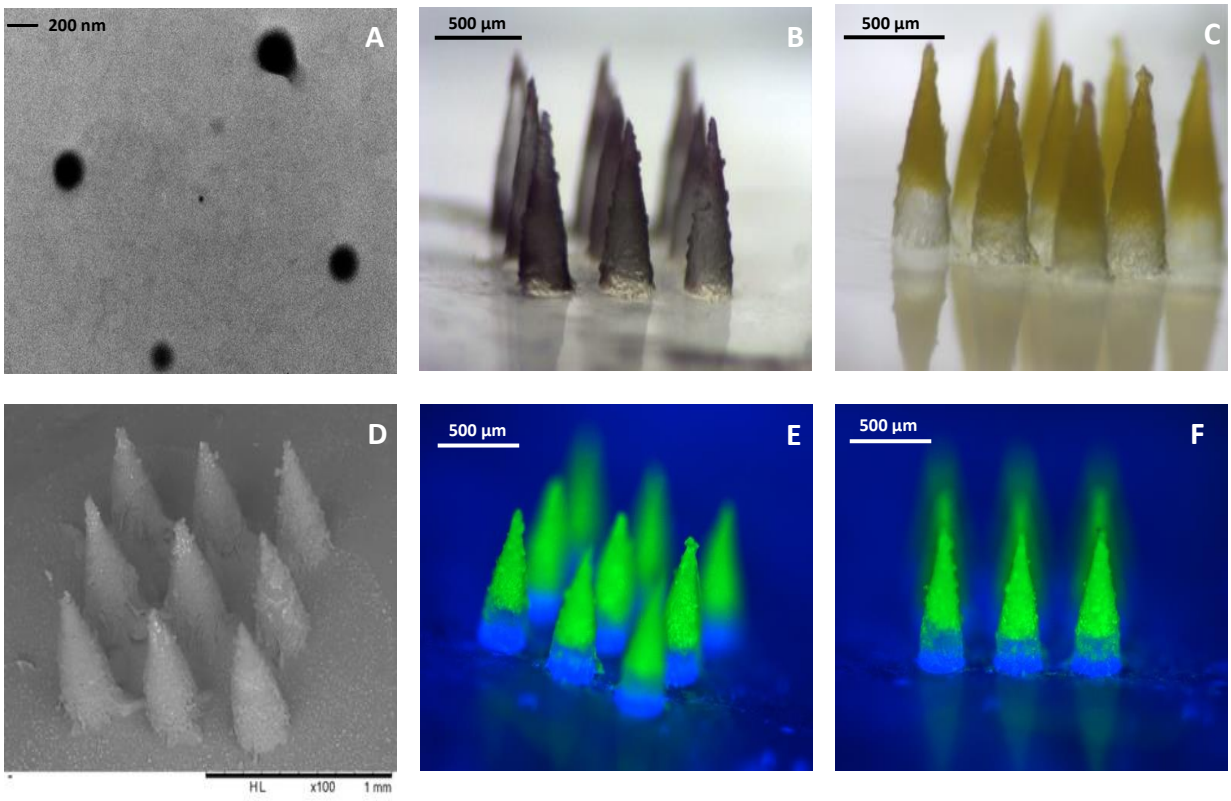

Fig. 7. Microscopic images of NPs and NP-loaded bilayer MN arrays: (A) TEM image of OVA NPs; digital light microscopic images of (B) OVA NP-loaded bilayer MN array and (C) FITC-OVA NP-loaded bilayer MN array; (D) SEM image of OVA NP-loaded MN array; (E, F) fluorescence microscopic images of FITC-OVA NP-loaded bilayer MN arrays with FITC-OVA NP (green colour) in needle part and the polymeric matrix (blue colour) in the bottom part.

3.6 Physical characterisation of bilayer MN arrays

Sufficient MN mechanical strength is crucial for successful payload delivery to the posterior segment of the eye because the MN must be strong enough to withstand compression forces

and penetrate the sclera without breaking. After the application of 3 N/array force, the height reduction for various formulations mentioned in Table 3 was determined to reflect the mechanical strength of bilayer MNs. The results are presented in Fig. 8A. Bilayer MNs fabricated from PVP with 40% w/w NP loading (M5) was seen as the optimal formulation as it achieved the purpose of encapsulating the highest possible amount of OVA, with less than 20% reduction of height after compression [69]. The result of MN formulation M1, M2 and M3, which all contained the mixture of PVP and PVA, suggested that after increasing the loading content of PLGA NPs from 20% to 30%, the height reduction was notably improved from approximately 13% to 28% ($p < 0.05$), indicating the enhancement of PLGA NP loading induced a reduction in mechanical strength of MN arrays. In addition, bilayer MNs fabricated from PVA (M6) exhibited the highest reduction (> 30%), indicating poor mechanical properties. Thus, Formulation M5 (40% w/w of OVA NP; 20% w/w of PVP and 40% w/w water) was selected for further insertion and dissolution property characterisation.

As mentioned in previous studies, the sclera played an important role in the transscleral permeation of therapeutics, especially macromolecules [9,10], indicating that scleral insertion and puncture are critical for the effective delivery of proteins. Accordingly, the insertion test of bilayer MNs was conducted to ascertain the insertion depth of bilayer MNs after applying a force of 3 N/array. Fig. 8B shows the OCT image of insertion for the optimised bilayer MN formulation (M5) in the porcine sclera. It reflected that the needle-part of MN arrays was successfully inserted into the excised porcine sclera, with an insertion depth of 569.36 ± 15.31 µm, which accounts for approximately 76% of the total MN height. Importantly, because of the viscoelasticity of scleral tissue, it is challenging to fully insert the needles into the administration site, which was consistent with the previous study [32]. However, taking advantage of bilayer MNs, the tip-part containing the NPs was completely inserted into the target tissue. This manufacturing approach not only minimises drug waste but also restricts the deposition of polymer matrix into the eye and finally reduces the risk of blurred vision. The bilayer MNs were completely dissolved within 3 min of insertion (data not shown), indicating that the optimised bilayer MN arrays can provide rapid dissolution in the sclera. The dissolution profiles of dissolving MNs exhibit a crucial effect on ocular drug delivery. If they dissolve too fast, the sharp-tips of MN arrays are likely to be dissolved before complete penetration into the scleral tissue, whilst if they dissolve too slowly may lead to poor patient compliance [70].

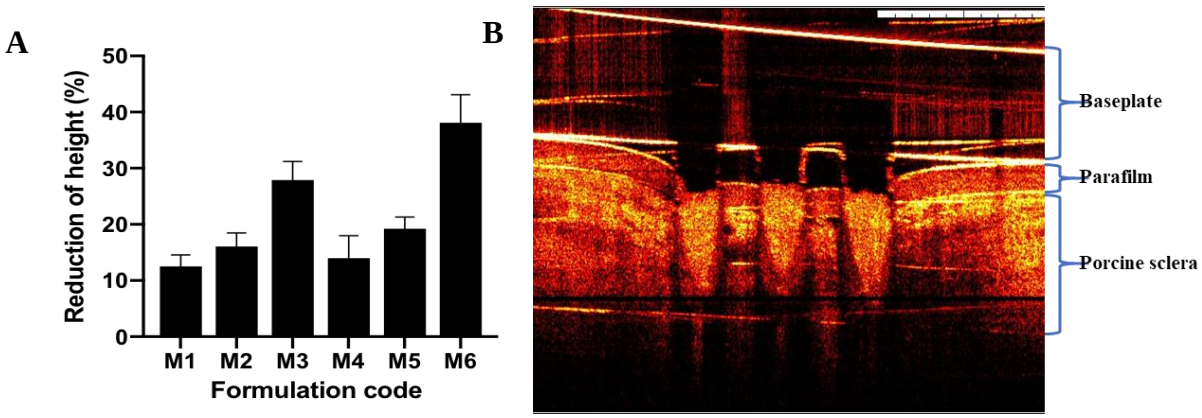

Fig. 8. Physical characteristics of bilayer MNs: (A) comparison of the height reduction of needles on the arrays formulated containing OVA NPs (means ± SD, n=3); (B) The OCT image of bilayer MN array following insertion into the porcine scleral tissue. The white scale bar represents a length of 1 mm.

3.7 Ex vivo sclera distribution study

MPM is an advanced fluorescence imaging technique that is capable of three-dimensional (3D) imaging of the biological tissue with a large thickness (2 mm) and reduced phototoxicity in live tissue [71]. Porcine scleral tissue with a thickness of approximately 750 μm was visualised by MPM to reflect the penetration of fluorescence-labelled OVA delivered through different treatments.

Fig. 9A indicates that the bilayer MN array (3 × 3 tips) successfully punctured the scleral tissue and induced 9 holes on its surface. The distribution of FITC-OVA within the sclera after different time intervals in three treatment groups is presented in Fig. 9B. In the NP suspension group, FITC-OVA NPs penetrated the scleral tissue very sparsely and superficially with maximum depths of 80, 150 and 250 μm at 1, 6 and 24 h, respectively, indicating the poor permeability of OVA NPs administrated by the eye drop. This observation was consistent with our group's previous investigation, in which the topically applied large molecule (Fluorescein isothiocyanate-dextran with MW of 70 kDa) was found to accumulate on the outer surface of the sclera [32]. After loading NPs into dissolving MNs, the maximum penetration depth of OVA within 24 h was considerably increased to about 550 μm and more drug retention in the sclera was observed. Compared with NP-loaded MNs, a slightly higher diffusion coefficient was observed in the FITC-OVA directly loaded MNs. In this group, after 24 h incubation, most of the payload was delivered to the bottom part of the sclera with a penetration depth up to 700 μm. This difference between the penetration depth of NP-loaded MN and OVA-loaded MN is

possibly due to the small size of plain OVA as well as the size-dependent permeability characteristics of the scleral tissue, resulting in a higher diffusion coefficient of plain OVA in the sclera [10,71]. This result may also suggest the poor movement and weak dynamic clearance of NPs in the sclera. Overall, the MPM results indicated that the introduction of the MN exhibited a comprehensive influence on promoting the transscleral delivery of NPs and macromolecules compared to conventional routes (e.g., eye drops), as a higher distribution depth and more drug retention in the scleral tissue were observed. Furthermore, in comparison with macromolecules directly delivered by MN arrays, the drugs delivered using NP-loaded MN arrays are anticipated to exhibit a longer lag-time in the sclera and sustain the release of encapsulated drugs.

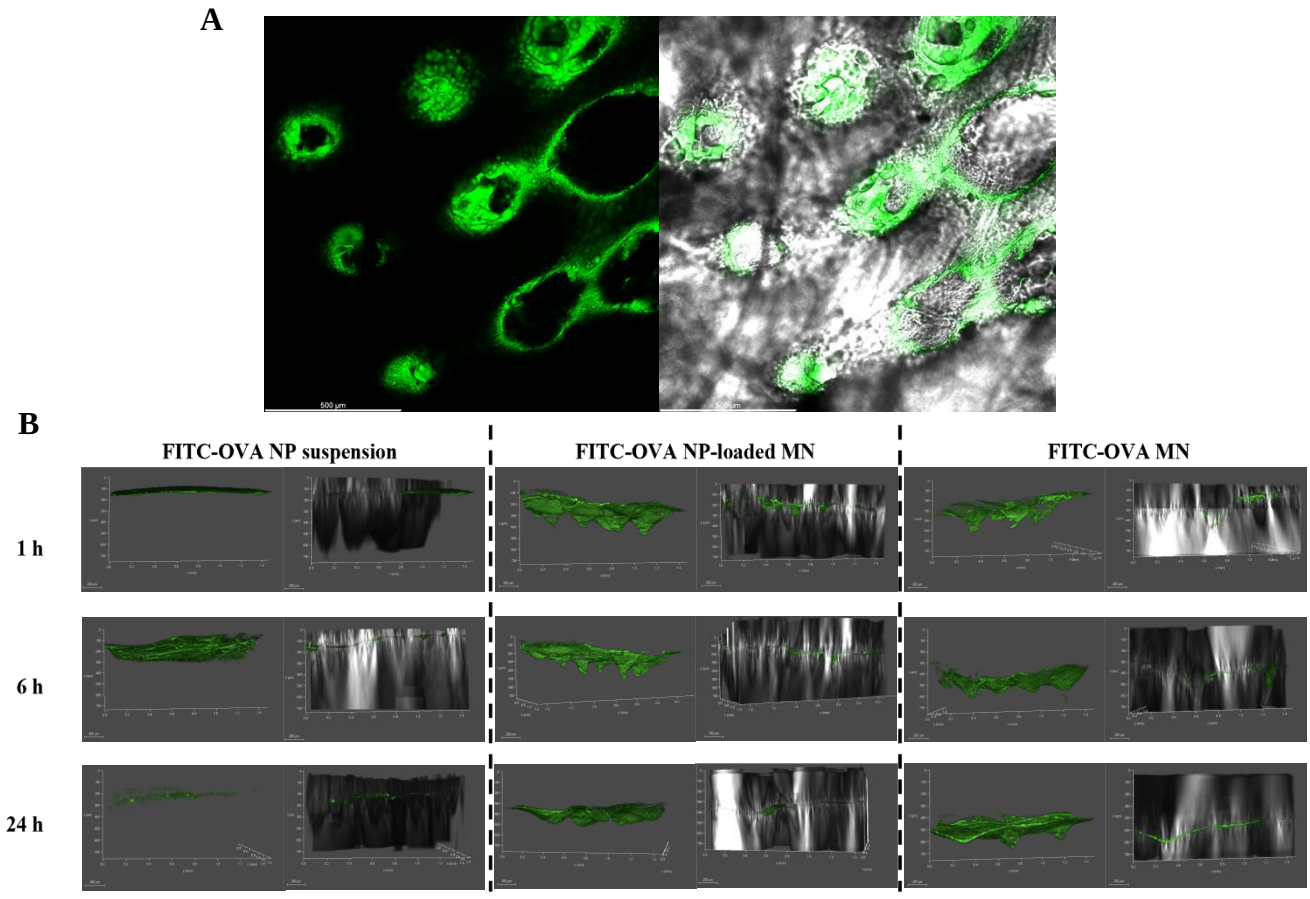

Fig. 9. The multiphoton microscopic images of FITC-OVA penetration in the porcine sclera and FITC-OVA was green labelled. (A) The surface image of sclera following the application of FITC-OVA NP-loaded MN array. Scale bar = 500 μm. (B) 3D visualisations of FITC-OVA and FITC-OVA NP penetration in porcine sclera within different treatment groups (FITC-OVA NP suspension, FITC-OVA NP-loaded MN, FITC-OVA loaded MN) at specific intervals (1, 6 and 24 h).

3.8 Biocompatibility studies

Following the application of NP-loaded MNs, both the polymers and NPs will be deposited into the eye. Therefore, it is essential to investigate whether the polymers and NPs are biocompatible for intraocular delivery before further *in vivo* studies. The viability of ARPE-19 cells after incubation with all polymers and NPs at various concentrations was found to be > 80% (Fig. 10). This not only demonstrated a high survival rate of the cells but also suggested that OVA NPs and bilayer MNs are likely to be non-toxic and biocompatible to ocular tissues, according to the ISO biological evaluation of medical devices Part 6 [72].

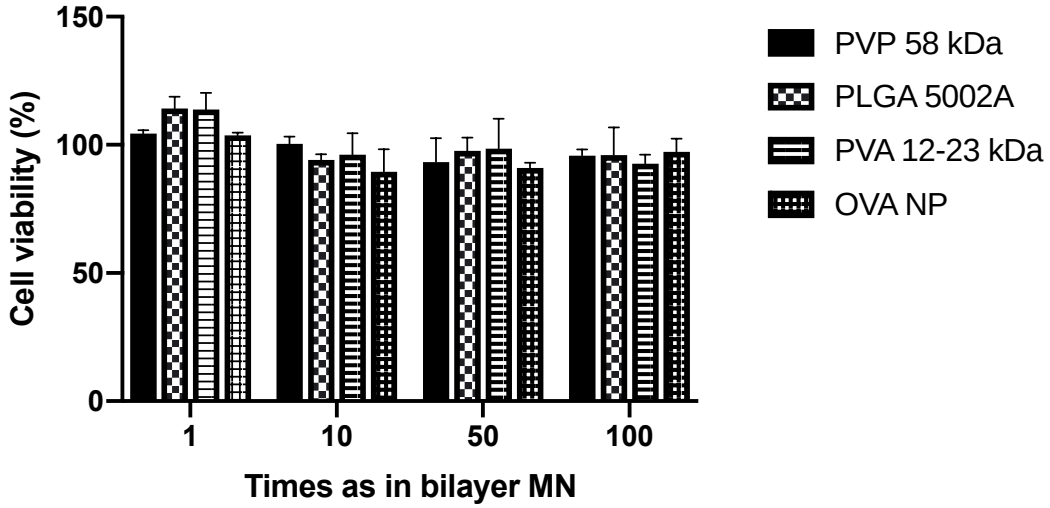

Fig. 10. Viability of ARPE-19 cells cultured with polymers (PVP, PVA and PLGA) employed in preparing bilayer MNs as well as OVA NPs at the concentrations in the equivalence of 1, 10, 50 and 100 times of them in each bilayer MN array (mean ± SD, n=3).

4. Conclusion

The combination of PLGA NPs and rapidly dissolving MNs for sustained and minimally invasive transscleral protein delivery to treat the posterior segment of ocular diseases was demonstrated for the first time. The formulation of model protein-loaded NP was optimised to sustain the release of the encapsulated protein for more than two months with high structural integrity and bioactivity. Furthermore, the optimised PLGA NPs were specifically deposited into the tips of MNs to form bilayer MNs in order to improve the cost-effectiveness of loading highly expensive and potent anti-VEGF biotherapeutics. *Ex vivo* studies suggested that the design of this NP-loaded MN system resulted in enhanced distribution depth and retention time of PLGA NPs in the scleral tissue. This protein encapsulated NP-loaded bilayer MN is likely

to provide an effective alternative compared to highly invasive hypodermic needles in alleviating retinal diseases and improve patient compliance. In the future, the anti-VEGF agents will be delivered *via* this platform and investigated in the context of *in vivo* efficacy, to further develop this novel delivery approach.

5. References

[1] P.A. Campochiaro, Ocular neovascularization, in: Angiogenes. An Integr. Approach From Sci. to Med., 2008. https://doi.org/10.1007/978-0-387-71518-6_44.

[2] D. Waite, Y. Wang, D. Jones, A. Stitt, T.R. Raj Singh, Posterior drug delivery via periocular route: Challenges and opportunities, Ther. Deliv. (2017). https://doi.org/10.4155/tde-2017-0097.

[3] J.N.S. Hiral J Shah, Nanoparticulate Transscleral Ocular Drug Delivery, J. Biomol. Res. Ther. (2014). https://doi.org/10.4172/2167-7956.1000116.

[4] M. Rodríguez Ramírez, M.I. del Barrio Manso, M.D. Martín Sánchez, Intravitreal injections: What do patients prefer? Analysis of patient's satisfaction and preferences about where to perform intravitreal injections, Arch. La Soc. Española Oftalmol. (English Ed. 89 (2014) 477–483. https://doi.org/https://doi.org/10.1016/j.oftale.2014.11.010.

[5] A. Luaces-Rodríguez, C. Mondelo-García, I. Zarra-Ferro, M. González-Barcia, P. Aguiar, A. Fernández-Ferreiro, F.J. Otero-Espinar, Intravitreal anti-VEGF drug delivery systems for age-related macular degeneration, Int. J. Pharm. 573 (2020) 118767. https://doi.org/10.1016/j.ijpharm.2019.118767.

[6] T.W. Olsen, S.Y. Aaberg, D.H. Geroski, H.F. Edelhauser, Human sclera: Thickness and surface area, Am. J. Ophthalmol. (1998). https://doi.org/10.1016/S0002-9394(99)80096-8.

[7] D. Huang, L. Wang, Y. Dong, X. Pan, G. Li, C. Wu, A novel technology using transscleral ultrasound to deliver protein loaded nanoparticles, Eur. J. Pharm. Biopharm. (2014). https://doi.org/10.1016/j.ejpb.2014.04.011.

[8] F.J.E. R.V. Fernandez, V.D. Tome, A.L. Rodriguez, A.C. Penedo, X.G. Otero, A.L. Alvarez, A.F. Ferreiro, Drug delivery to the posterior segmnet of the eye: biopharmaceutic and pharmacokinetics considerations, (2020).

[9] J. Ambati, C.S. Canakis, J.W. Miller, E.S. Gragoudas, A. Edwards, D.J. Weissgold, I. Kim, F.C. Delori, A.P. Adamis, Diffusion of high molecular weight compounds through sclera, Investig. Ophthalmol. Vis. Sci. (2000).

[10] H. Wen, J. Hao, S.K. Li, Characterization of human sclera barrier properties for transscleral delivery of bevacizumab and ranibizumab, J. Pharm. Sci. (2013). https://doi.org/10.1002/jps.23387.

[11] S. Kulkarni, S.P. Gupta, N. Upmanyu, S.D. Tonpay, Solubility enhancement of water insoluble drug for ophthalmic formulation, Int. J. Drug Deliv. (2011). https://doi.org/10.5138/ijdd.2010.0975.0215.03064.

[12] X. Qu, V. V. Khutoryanskiy, A. Stewart, S. Rahman, B. Papahadjopoulos-Sternberg, C. Dufes, D. McCarthy, C.G. Wilson, R. Lyons, K.C. Carter, A. Schätzlein, I.F. Uchegbu, Carbohydrate-based micelle clusters which enhance hydrophobic drug bioavailability by up to 1 order of magnitute, Biomacromolecules. (2006). https://doi.org/10.1021/bm0604000.

[13] M.E. Myles, D.M. Neumann, J.M. Hill, Recent progress in ocular drug delivery for posterior segment disease: Emphasis on transscleral iontophoresis, Adv. Drug Deliv. Rev. (2005). https://doi.org/10.1016/j.addr.2005.08.006.

[14] J.H. Jung, B. Chiang, H.E. Grossniklaus, M.R. Prausnitz, Ocular drug delivery targeted by iontophoresis in the suprachoroidal space using a microneedle, J. Control. Release. (2018). https://doi.org/10.1016/j.jconrel.2018.03.001.

[15] A.S. Rzhevskiy, T.R.R. Singh, R.F. Donnelly, Y.G. Anissimov, Microneedles as the technique of drug delivery enhancement in diverse organs and tissues, J. Control. Release. (2018). https://doi.org/10.1016/j.jconrel.2017.11.048.

[16] A.S. Cordeiro, I.A. Tekko, M.H. Jomaa, L. Vora, E. McAlister, F. Volpe-Zanutto, M. Nethery, P.T. Baine, N. Mitchell, D.W. McNeill, R.F. Donnelly, Two-Photon Polymerisation 3D Printing of Microneedle Array Templates with Versatile Designs: Application in the Development of Polymeric Drug Delivery Systems, Pharm. Res. 37 (2020) 174. https://doi.org/10.1007/s11095-020-02887-9.

[17] R.F. Donnelly, R. Majithiya, T. Raghu, R. Singh, D.I.J. Morrow, M.J. Garland, Y.K. Demir, E. Ryan, D. Gillen, C.J. Scott, A.D. Woolfson, Design , Optimization and Characterisation of Polymeric Microneedle Arrays Prepared by a Novel Laser-Based Micromoulding Technique, (2011) 41–57. https://doi.org/10.1007/s11095-010-0169-8.

[18] L.K. Vora, K. Moffatt, I.A. Tekko, A.J. Paredes, F. Volpe-Zanutto, D. Mishra, K. Peng, R. Raj Singh Thakur, R.F. Donnelly, Microneedle array systems for long-acting drug delivery, Eur. J. Pharm. Biopharm. 159 (2021) 44–76. https://doi.org/https://doi.org/10.1016/j.ejpb.2020.12.006.

[19] L.K. Vora, A.J. Courtenay, I.A. Tekko, E. Larrañeta, R.F. Donnelly, Pullulan-based dissolving microneedle arrays for enhanced transdermal delivery of small and large biomolecules, Int. J. Biol. Macromol. 146 (2020) 290–298. https://doi.org/10.1016/j.ijbiomac.2019.12.184.

[20] Á. Cárcamo-Martínez, B. Mallon, J. Domínguez-Robles, L.K. Vora, Q.K. Anjani, R.F. Donnelly, Hollow microneedles: A perspective in biomedical applications, Int. J. Pharm. 599 (2021) 120455. https://doi.org/https://doi.org/10.1016/j.ijpharm.2021.120455.

[21] K. McAvoy, D. Jones, R.R.S. Thakur, Synthesis and Characterisation of Photocrosslinked poly(ethylene glycol) diacrylate Implants for Sustained Ocular Drug Delivery, Pharm. Res. (2018). https://doi.org/10.1007/s11095-017-2298-9.

[22] A.J. Paredes, I.K. Ramöller, P.E. McKenna, M.T.A. Abbate, F. Volpe-Zanutto, L.K. Vora, M. Kilbourne-Brook, C. Jarrahian, K. Moffatt, C. Zhang, I.A. Tekko, R.F. Donnelly, Microarray patches: Breaking down the barriers to contraceptive care and HIV prevention for women across the globe, Adv. Drug Deliv. Rev. 173 (2021) 331–348. https://doi.org/https://doi.org/10.1016/j.addr.2021.04.002.

[23] M.S. Muthu, Nanoparticles based on PLGA and its co-polymer: An overview, Asian J. Pharm. (2009). https://doi.org/10.4103/0973-8398.59948.

[24] N. Elsaid, T.L. Jackson, Z. Elsaid, A. Alqathama, S. Somavarapu, PLGA microparticles entrapping chitosan-based nanoparticles for the ocular delivery of ranibizumab, Mol. Pharm. (2016). https://doi.org/10.1021/acs.molpharmaceut.6b00335.

[25] E. Larrañeta, L. Vora, Delivery of Nanomedicines Using Microneedles, Microneedles Drug Vaccine Deliv. Patient Monit. (2018) 177–205. https://doi.org/doi:10.1002/9781119305101.ch6.

[26] C.R. Osswald, J.J. Kang-Mieler, Controlled and Extended Release of a Model Protein from a Microsphere-Hydrogel Drug Delivery System, Ann. Biomed. Eng. (2015). https://doi.org/10.1007/s10439-015-1314-7.

[27] M. Zaric, O. Lyubomska, O. Touzelet, C. Poux, S. Al-Zahrani, F. Fay, L. Wallace, D. Terhorst, B. Malissen, S. Henri, U.F. Power, C.J. Scott, R.F. Donnelly, A. Kissenpfennig, Skin dendritic cell targeting via microneedle arrays laden with antigen-encapsulated poly- D, l -Lactide- Co -Glycolide nanoparticles induces efficient antitumor and antiviral immune responses, ACS Nano. 7 (2013) 2042–2055. https://doi.org/10.1021/nn304235j.

[28] J. Mönkäre, M. Pontier, E.E.M. van Kampen, G. Du, M. Leone, S. Romeijn, M.R. Nejadnik, C. O'Mahony, B. Slütter, W. Jiskoot, J.A. Bouwstra, Development of PLGA nanoparticle loaded dissolving microneedles and comparison with hollow microneedles in intradermal vaccine delivery, Eur. J. Pharm. Biopharm. 129 (2018) 111–121. https://doi.org/10.1016/j.ejpb.2018.05.031.

[29] J.L. Cleland, A.J.S. Jones, Stable formulations of recombinant human growth hormone and interferon-γ for microencapsulation in biodegradable microspheres, Pharm. Res. (1996). https://doi.org/10.1023/A:1016063109373.

[30] M. Morlock, H. Koll, G. Winter, T. Kissel, Microencapsulation of rh-erythropoietin, using biodegradable poly(D,L- lactide-co-glycolide): Protein stability and the effects of stabilizing excipients, Eur. J. Pharm. Biopharm. (1997). https://doi.org/10.1016/S0939-6411(96)00017-3.

[31] H. Sah, Stabilization of proteins against methylene chloride/water interface-induced denaturation and aggregation, J. Control. Release. (1999). https://doi.org/10.1016/S0168-3659(98)00148-5.

[32] R.R.S. Thakur, I.A. Tekko, F. Al-Shammari, A.A. Ali, H. McCarthy, R.F. Donnelly, Rapidly dissolving polymeric microneedles for minimally invasive intraocular drug delivery, Drug Deliv. Transl. Res. (2016). https://doi.org/10.1007/s13346-016-0332-9.

[33] D. Ramadon, A.D. Permana, A.J. Courtenay, M.T.C. McCrudden, I.A. Tekko, E. McAlister, Q.K. Anjani, E. Utomo, H.O. McCarthy, R.F. Donnelly, Development, Evaluation, and Pharmacokinetic Assessment of Polymeric Microarray Patches for Transdermal Delivery of Vancomycin Hydrochloride, Mol. Pharm. 17 (2020) 3353–3368. https://doi.org/10.1021/acs.molpharmaceut.0c00431.

[34] P. Blasi, Poly(lactic acid)/poly(lactic-co-glycolic acid)-based microparticles: an overview, J. Pharm. Investig. 49 (2019) 337–346. https://doi.org/10.1007/s40005-019-00453-z.

[35] Y.Y. Yang, T.S. Chung, N. Ping Ng, Morphology, drug distribution, and in vitro release profiles of biodegradable polymeric microspheres containing protein fabricated by double-emulsion solvent extraction/evaporation method, Biomaterials. (2001). https://doi.org/10.1016/S0142-9612(00)00178-2.

[36] S.Y. Xie, S.L. Wang, B.K. Zhao, C. Han, M. Wang, W.Z. Zhou, Effect of PLGA as a polymeric emulsifier on preparation of hydrophilic protein-loaded solid lipid nanoparticles, Colloids Surfaces B Biointerfaces. (2008). https://doi.org/10.1016/j.colsurfb.2008.08.018.

[37] S. Mohammadi-Samani, B. Taghipour, PLGA micro and nanoparticles in delivery of peptides and proteins; Problems and approaches, Pharm. Dev. Technol. (2015).

https://doi.org/10.3109/10837450.2014.882940.
[38] S. Son, W.R. Lee, Y.K. Joung, M.H. Kwon, Y.S. Kim, K.D. Park, Optimized stability retention of a monoclonal antibody in the PLGA nanoparticles, Int. J. Pharm. (2009). https://doi.org/10.1016/j.ijpharm.2008.09.061.
[39] Š. Peternel, R. Komel, Isolation of biologically active nanomaterial (inclusion bodies) from bacterial cells, Microb. Cell Fact. (2010). https://doi.org/10.1186/1475-2859-9-66.
[40] G. Jiang, B.H. Woo, F. Kang, J. Singh, P.P. DeLuca, Assessment of protein release kinetics, stability and protein polymer interaction of lysozyme encapsulated poly(D,L-lactide-co-glycolide) microspheres, J. Control. Release. (2002). https://doi.org/10.1016/S0168-3659(01)00533-8.
[41] T. Verrecchia, P. Huve, D. Bazile, M. Veillard, G. Spenlehauer, P. Couvreur, Adsorption/desorption of human serum albumin at the surface of poly(lactic acid) nanoparticles prepared by a solvent evaporation process, J. Biomed. Mater. Res. (1993). https://doi.org/10.1002/jbm.820270807.
[42] S.P. Schwendeman, M. Cardamone, A. Klibanov, R. Langer, M.R. Brandon, Stability of Proteins and Their Delivery from Biodegradable Polymer Microspheres, in: Microparticulate Syst. Deliv. Proteins Vaccines, 2020. https://doi.org/10.1201/9781003067542-1.
[43] M. Van De Weert, W.E. Hennink, W. Jiskoot, Protein instability in poly(lactic-co-glycolic acid) microparticles, Pharm. Res. (2000). https://doi.org/10.1023/A:1026498209874.
[44] I.J. Castellanos, G. Cruz, R. Crespo, K. Griebenow, Encapsulation-induced aggregation and loss in activity of γ-chymotrypsin and their prevention, J. Control. Release. (2002). https://doi.org/10.1016/S0168-3659(02)00073-1.
[45] F. Kang, G. Jiang, A. Hinderliter, P.P. Deluca, J. Singh, Lysozyme stability in primary emulsion for PLGA microsphere preparation: Effect of recovery methods and stabilizing excipients, Pharm. Res. (2002). https://doi.org/10.1023/A:1015354028908.
[46] P. Johansen, Y. Men, R. Audran, G. Corradin, H.P. Merkle, B. Gander, Improving stability and release kinetics of microensapsulated tetanus toxoid by co-encapsulation of additives, Pharm. Res. (1998). https://doi.org/10.1023/A:1011998615267.
[47] S. Sharif, D.T. O'Hagan, A comparison of alternative methods for the determination of the levels of proteins entrapped in poly(lactide-co-glycolide) microparticles, Int. J. Pharm. (1995). https://doi.org/10.1016/0378-5173(94)00318-Y.
[48] M. Van De Weert, J. Hoechstetter, W.E. Hennink, D.J.A. Crommelin, The effect of a water/organic solvent interface on the structural stability of lysozyme, J. Control. Release. (2000). https://doi.org/10.1016/S0168-3659(00)00277-7.
[49] E.S. Lee, M.J. Kwon, H. Lee, J.J. Kim, Stabilization of protein encapsulated in poly(lactide-co-glycolide) microspheres by novel viscous S/W/O/W method, Int. J. Pharm. (2007). https://doi.org/10.1016/j.ijpharm.2006.09.008.
[50] J.C. Stanwick, M.D. Baumann, M.S. Shoichet, Enhanced neurotrophin-3 bioactivity and release from a nanoparticle-loaded composite hydrogel, J. Control. Release. (2012). https://doi.org/10.1016/j.jconrel.2012.03.024.
[51] C. Sturesson, J. Carlfors, Incorporation of protein in PLG-microspheres with retention of bioactivity, J. Control. Release. (2000). https://doi.org/10.1016/S0168-3659(00)00205-4.
[52] H. Sah, Protein behavior at the water/methylene chloride interface, J. Pharm. Sci. (1999). https://doi.org/10.1021/js9900654.
[53] and S.D.P. O. L. Johnson, W. Jaworowicz, J. L. Cleland, L. Bailey, M. Char- nis, E. Duenas, C. Wu, D. Shepard, S. Magil, T. Last, A. J. S. Jones, The stabilization of human growth hor- mone into biodegradable microspheres.pdf, (1997) 14:730–735.
[54] L. Vora, M. Tyagi, K. Patel, S. Gupta, P. Vavia, Self-assembled nanocomplexes of anionic pullulan and polyallylamine for DNA and pH-sensitive intracellular drug delivery, J. Nanoparticle Res. (2014). https://doi.org/10.1007/s11051-014-2781-8.
[55] K. Patel, M. Tyagi, J. Monpara, L. Vora, S. Gupta, P. Vavia, Arginoplexes: an arginine-anchored nanoliposomal carrier for gene delivery, J. Nanoparticle Res. 16 (2014) 2345. https://doi.org/10.1007/s11051-014-2345-y.
[56] C. Sturesson, P. Artursson, R. Ghaderi, K. Johansen, A. Mirazimi, I. Uhnoo, L. Svensson, A.C. Albertsson, J. Carlfors, Encapsulation of rotavirus into poly(lactide-co-glycolide) microspheres, J. Control. Release. (1999). https://doi.org/10.1016/S0168-3659(99)00014-0.
[57] D.T. O'Hagan, J.P. McGee, R. Boyle, D. Gumaer, X.M. Li, B. Potts, C.Y. Wang, W.C. Koff, The preparation, characterization and pre-clinical evaluation of an orally administered HIV-I vaccine, consisting of a branched peptide immunogen entrapped in controlled release microparticles, J. Control. Release. (1995). https://doi.org/10.1016/0168-3659(95)00052-A.
[58] L. Vora, S. V G, P. Vavia, Zero order controlled release delivery of cholecalciferol from injectable biodegradable microsphere: In-vitro characterization and in-vivo pharmacokinetic studies, Eur. J.

Pharm. Sci. 107 (2017) 78–86. https://doi.org/10.1016/j.ejps.2017.06.027.
[59] M.F. Zambaux, F. Bonneaux, R. Gref, E. Dellacherie, C. Vigneron, Preparation and characterization of protein C-loaded PLA nanoparticles, J. Control. Release. 60 (1999) 179–188. https://doi.org/10.1016/S0168-3659(99)00073-5.
[60] M. Igartua, R.M. Hernández, A. Esquisabel, A.R. Gascón, M.B. Calvo, J.L. Pedraz, Stability of BSA encapsulated into PLGA microspheres using page and capillary electrophoresis, Int. J. Pharm. 169 (1998) 45–54. https://doi.org/10.1016/S0378-5173(98)00101-X.
[61] G. Zhu, S.R. Mallery, S.P. Schwendeman, Stabilization of proteins encapsulated in injectable poly (lactide-co- glycolide), Nat. Biotechnol. 18 (2000) 52–57. https://doi.org/10.1038/71916.
[62] R.L. K. Fu, D.W. Pack, A.M. Klibanov, Visual Evidence of Acidic Environment Within Degrading Poly(lactic-co-glycolic acid) (PLGA) Microspheres, Pharm. Res. 17 (2000). https://doi.org/10.1023/A.
[63] M. Vert, S. Li, H. Garreau, More about the degradation of LA/GA-derived matrices in aqueous media, J. Control. Release. 16 (1991) 15–26. https://doi.org/10.1016/0168-3659(91)90027-B.
[64] A.G. Ding, S.P. Schwendeman, Acidic microclimate pH Distribution in PLGA microspheres monitored by confocal laser scanning microscopy, Pharm. Res. 25 (2008) 2041–2052. https://doi.org/10.1007/s11095-008-9594-3.
[65] Q.L. Wang, D.D. Zhu, X.B. Liu, B.Z. Chen, X.D. Guo, Microneedles with controlled bubble sizes and drug distributions for efficient transdermal drug delivery, Sci. Rep. (2016). https://doi.org/10.1038/srep38755.
[66] page 10. Lucentis US Prescribing Information 2013, 125156s081lbl-DME.pdf, (2013) 3–17.
[67] S. Friedrich, Y.L. Cheng, B. Saville, Drug distribution in the vitreous humor of the human eye: The effects of intravitreal injection position and volume, Curr. Eye Res. 16 (1997) 663–669. https://doi.org/10.1076/ceyr.16.7.663.5061.
[68] D. Malik, M. Tarek, J.C. Del Carpio, C. Ramirez, D. Boyer, M.C. Kenney, B.D. Kuppermann, Safety profiles of anti-VEGF drugs: Bevacizumab, ranibizumab, aflibercept and ziv-aflibercept on human retinal pigment epithelium cells in culture, Br. J. Ophthalmol. 98 (2014) 10–16. https://doi.org/10.1136/bjophthalmol-2014-305302.
[69] L.K. Vora, R.F. Donnelly, E. Larrañeta, P. González-Vázquez, R.R.S. Thakur, P.R. Vavia, Novel bilayer dissolving microneedle arrays with concentrated PLGA nano-microparticles for targeted intradermal delivery: Proof of concept, J. Control. Release. (2017). https://doi.org/10.1016/j.jconrel.2017.10.005.
[70] S.P. Sullivan, N. Murthy, M.R. Prausnitz, Minimally invasive protein delivery with rapidly dissolving polymer microneedles, Adv. Mater. (2008). https://doi.org/10.1002/adma.200701205.
[71] R.K.P. Benninger, D.W. Piston, Two-photon excitation microscopy for unit 4.11 the study of living cells and tissues, Curr. Protoc. Cell Biol. (2013). https://doi.org/10.1002/0471143030.cb0411s59.
[72] D.H. Geroski, H.F. Edelhauser, Transscleral drug delivery for posterior segment disease, Adv. Drug Deliv. Rev. (2001). https://doi.org/10.1016/S0169-409X(01)00193-4.
[72] International Organisation for Standardisation (ISO): Biological Evaluation of Medical Devices-Part 6: Test for Local Effects after Implantation, ISO 10993-6. (1994).

Supplementary section

Table S1. The lyophilisation cycle for NP drying.

Step	Temperature (˚C)	Pressure (torr)	Time (min)	Type of step
1	5	150	10	Hold
2	-40	150	180	Hold
3	-35	190	300	Ramp/Hold
4	-30	190	300	Ramp/Hold
5	-25	190	300	Ramp/Hold
6	-20	190	300	Ramp/Hold
7	-15	190	300	Ramp/Hold

8	-10	190	180	Ramp
9	-10	600	120	Hold
10	20	600	50	Hold

Table S2. Particle size, PDI and zeta potential of the optimised OVA NP before and after lyophilisation (means ± SD, n=3).

Optimised OVA NP	NP size (nm)	PDI	Zeta potential (mV)
Before lyophilisation	242.1 ± 13.55	0.133 ± 0.028	-8.68 ± 1.18
After lyophilisation	265.9 ± 21.98	0.163 ± 0.023	-7.98 ± 0.71